J. Am. Soc. Mass Spectrom. (2016) 27:1483–1490
DOI: 10.1007/s13361-016-1427-8

RESEARCH ARTICLE

Photo and Collision Induced Isomerization of a Cyclic Retinal Derivative: An Ion Mobility Study

Neville J. A. Coughlan,[1] Michael S. Scholz,[1] Christopher S. Hansen,[2] Adam J. Trevitt,[2] Brian D. Adamson,[1] Evan J. Bieske[1]

[1]School of Chemistry, University of Melbourne, Melbourne, Australia
[2]School of Chemistry, University of Wollongong, Wollongong, Australia

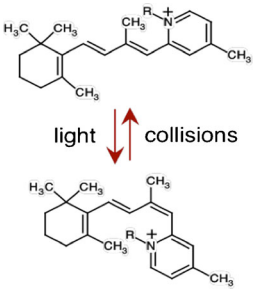

Abstract. A cationic degradation product, formed in solution from retinal Schiff base (RSB), is examined in the gas phase using ion mobility spectrometry, photoisomerization action spectroscopy, and collision induced dissociation (CID). The degradation product is found to be *N*-*n*-butyl-2-(β-ionylidene)-4-methylpyridinium (BIP) produced through 6π electrocyclization of RSB followed by protonation and loss of dihydrogen. Ion mobility measurements show that BIP exists as *trans* and *cis* isomers that can be interconverted through buffer gas collisions and by exposure to light, with a maximum response at λ = 420 nm.

Keywords: Retinal, Ion mobility, Photoisomerization, Ion spectroscopy, Collision induced isomerization

Received: 30 March 2016/Revised: 10 May 2016/Accepted: 20 May 2016/Published Online: 8 June 2016

Introduction

One of the more remarkable aspects of biology is that a single molecule can perform different functions according to its environment and context. One prominent example is retinal protonated Schiff base (RPSB), Scheme 1, which serves as the key photoactive molecule in the visual receptors of animals, and also as the primary light-activated molecule in proton and chloride ion pumps in microbes [1, 2]. In these contexts, the primary photoresponse is the structural rearrangement of the retinal molecule [3]. In vivo, the opsin-hosted RPSB chromophore is photostable, and is recycled for many visual phototransduction events. However, as light sensitive structures (e.g., eyes of vertebrates) age, the concentration of fluorescent lipofuscin granules associated with lysosomal digestion of the cell increases. The lipofuscin granules are known to contain several bisretinoid species including A2E and all-*trans* retinal dimer, which are formed from retinal through dimerization and condensation pathways. These pigments are associated with age-related macular degeneration and vision loss [4–6].

Degradation of RPSB also occurs outside the cellular environment. For example, it was recently shown that photofragmentation of RPSB in the gas phase produces the protonated Schiff base of β-ionone through elimination of toluene following intramolecular cyclization of the polyene chain [7, 8]. Other degradation mechanisms are important in solution. Okamura and coworkers investigated the 6π electrocyclization of retinal Schiff base (RSB) in C_6D_6 to form a dihydropyridine (DHP), Scheme 2, in a process that occurs more rapidly for 13-*cis* RSB than *trans* RSB [9]. As shown in Scheme 2, protonation of DHP might reasonably be expected to be followed by dihydrogen loss and formation of the BIP cation [*N*-*n*-butyl-2-(β-ionylidene)-4-methylpyridinium (*m/z* = 338)].

Our interest in the BIP cation was prompted by a recognition that although an acidified, fresh solution of RSB, when electrosprayed, produced mainly RPSB (*m/z* = 340), as the solution aged over several days, the main electrosprayed ion became one with *m/z* = 338 [7]. In the current study, we have investigated the *m/z* = 338 cation using ion mobility spectrometry (IMS), collision induced dissociation (CID) mass spectrometry, and density functional theory (DFT) calculations, confirming that it is indeed BIP. Furthermore, using ion mobility mass spectrometry, we demonstrate that BIP has *trans* and *cis* geometrical isomers that can be interconverted through

Electronic supplementary material The online version of this article (doi:10.1007/s13361-016-1427-8) contains supplementary material, which is available to authorized users.

Correspondence to: Evan J. Bieske; *e-mail:* evanjb@unimelb.edu.au

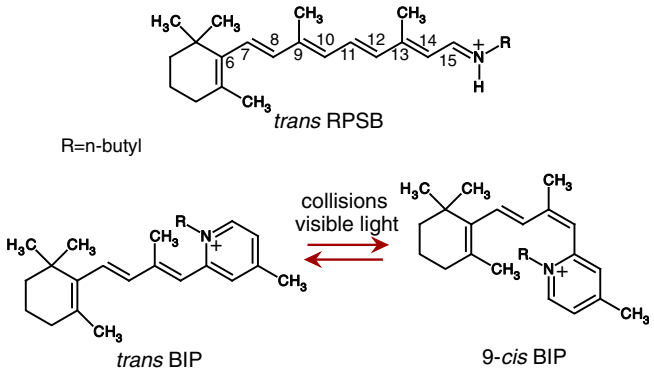

Scheme 1. Retinal protonated Schiff base (RPSB), and *trans* and *cis* isomers of *N*-*n*-butyl-2-(β-ionylidene)-4-methylpyridinium (BIP), which can be interconverted with UV/visible light or buffer gas collisions. Note that the displayed 9-*cis* BIP isomer is a representative *cis* isomer

absorption of visible/UV light or by collisions with N_2 buffer gas. The BIP cation has similar structural features to molecules that have been used in switching applications, including alkene derivatives, stilbenes, and azobenzenes, which rely on *trans-cis* isomerizations [10–12]. Because it is easy to generate from RPSB and can be reversibly photoisomerized, BIP may be appropriate as the core molecular unit for light-activated molecular machines.

Experimental

The *m/z* = 338 degradation product of RPSB was examined using a custom-built tandem ion mobility apparatus in which different isomers are separated according to their drift mobility and by their isomerization behavior following exposure to light [photoisomerization action (PISA) spectroscopy] or collisions

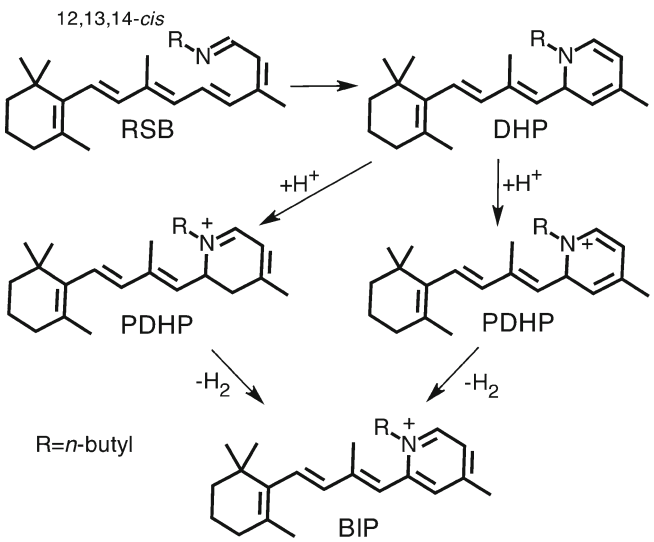

Scheme 2. Successive transformation of RSB to dihydropyridine (DHP), protonated dihydropyridine (PDHP), and *N*-*n*-butyl-2-(β-ionylidene)-4-methylpyridinium (BIP)

with buffer gas molecules [collision induced isomerization (CII)]. The tandem ion mobility spectrometer and photoisomerization action spectroscopy approach has been described previously, and further details are given below [13, 14]. High resolution CID mass spectra and MS^n spectra for BIP cations and fragment ions were collected using a Thermo Scientific (San Jose, Ca) XL Hybrid Ion Trap-Orbitrap mass spectrometer and a modified Thermo Scientific LTQ XL mass spectrometer, respectively. Details of the CID measurements are given in the Supporting Information.

Arrangements for the ion mobility experiments are illustrated in Figure 1. Briefly, electrosprayed cations, produced from an acidified 10^{-4} M solution of degraded RSB in methanol/water (electrospray voltage ≈ 3 kV, flow rate ≈ 10 μL/min, 2% acetic acid), were accumulated in an ion funnel before being launched in 100 μs pulses at 20 Hz into a 0.9 m drift tube filled with N_2 buffer gas (P ≈ 6.2 Torr, E = 44 V/cm). At the end of the drift tube, the ions were gathered radially by a second ion funnel before passing through a 0.3 mm orifice into an octopole ion guide from where they exit through a second 3 mm orifice into a quadrupole mass filter. Mass-selected ions were sensed by a channeltron detector connected to a discriminator and a multichannel scaler. The ions' arrival time distribution (ATD) was built up as a histogram of ion counts versus time. The mobility resolution for the BIP cations is typically $t_d/\Delta t_d$ = 70–80 [13]. Under the prevailing operating conditions, the effective temperature of the ions is predicted to be ≈310 K [15].

When operated in tandem IMS-photo-IMS mode, alternate ion packets were irradiated 7.5 mm after IG2 with light from a pulsed, tunable optical parametric oscillator (OPO, 10 Hz, λ = 320-710 nm, 10 ns pulse width, 5 cm^{-1} bandwidth). Photoisomerization is reflected in the difference between laser-on and laser-off ATDs. Care was taken to avoid saturating the electronic transitions. Typically, the pulse energy was 5–10 mJ/pulse and the beam cross section was 5 cm^2, corresponding to a fluence of 1–2 mJ/cm^2/pulse. At these light levels, photodissociation of the BIP ions was negligible. Note that we were unable to measure the photoisomerization response below 320 nm because of interference by background ions produced from photoionization of impurities in the drift gas.

The collisional excitation region (slammer) is situated 15 mm after IG2 and consists of two copper mesh electrodes separated by 3 mm between which an adjustable potential difference can be applied. For sufficiently high electric fields, collisions with N_2 buffer gas cause the BIP ions to isomerize between two different forms. Parent and daughter isomer ions are separated in the second drift region. As demonstrated by Clemmer and coworkers [16, 17], by monitoring CII as a function of the electric field strength, one can derive information on barrier heights for molecular rearrangements.

Normally, the potential difference between the slammer electrodes is 20 V, corresponding to an electric field of 60 V/cm. The electric field between the two electrodes was increased by raising the voltages on all upstream electrodes such that the electric fields throughout the rest of the instrument remained constant. Under normal operating conditions, the

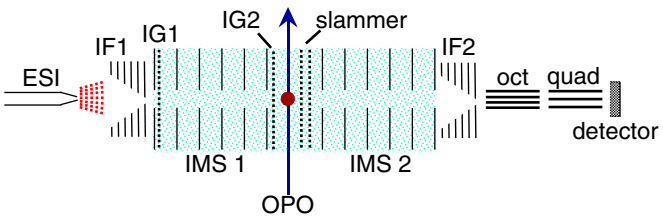

Figure 1. Tandem ion mobility spectrometer. Electrosprayed ions accumulate in the first ion funnel (IF1) and are periodically launched through an ion gate (IG1) into the first drift region (IMS 1) where they travel through N_2 buffer gas (P ≈ 6.2 Torr) propelled by an electric field (E ≈ 44 V cm^{-1}). The ions encounter a second ion gate (IG2) that can be opened to pass mobility-selected isomers. Immediately after IG2, ions can be irradiated with light from a tunable OPO. Alternatively, the ions can be energized in the collisional excitation region (slammer), where an adjustable potential difference is applied between grid electrodes separated by 3 mm. After traveling through the second drift region (IMS 2), the ions are collected by an ion funnel (IF2), and pass through an octopole and quadrupole mass filter before striking a detector

highest attainable potential difference between the slammer grids before electrical breakdown was 320 V.

RPSB was synthesized under exclusion of light in an Ar atmosphere according to previous methods [18]. *Trans* retinal (Sigma Aldrich, Sydney, Australia) was dissolved in excess *n*-butylamine (Sigma Aldrich) and allowed to react at 10 °C until ^{1}H NMR showed no evidence of the aldehyde carbonyl signal at ≈ 10 ppm. 2,4-Lutidine cations were electrosprayed from a 10^{-4} M solution of 2,4-lutidine (Sigma Aldrich, 99%) in a 1:1 mixture of methanol and H_2O with 0.2% acetic acid.

Results and Discussion

Formation of the m/z = 338 Cation

The *m/z* = 338 cation was observed whenever acidified RSB samples were electrosprayed, becoming more abundant as the solution aged, and eventually becoming the predominant ion. As shown in Figure 2, the ATD for the *m/z* = 338 cation exhibits two distinct peaks, labeled X and Y, having a ≈3:1 intensity ratio. The measured collision cross sections (Ω_m) for the two *m/z* = 338 isomers with N_2 are 8%–12% less than *trans* RPSB (isomer A), indicating that they have more compact structures. Indeed, their collision cross sections are similar to those of the RPSB isomers C' and D, which have been assigned to cyclic or triple-*cis* forms [18, 19]. Okamura et al. found that

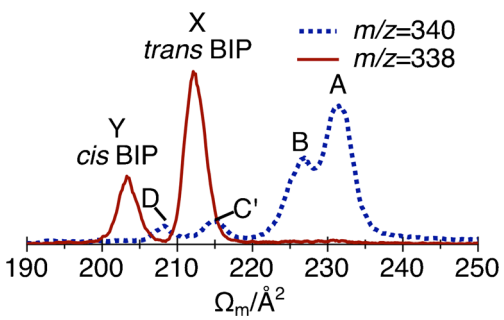

Figure 2. Ion mobility spectra of RPSB (*m/z* = 340) and BIP (*m/z* = 338) showing evidence for *trans* and *cis* BIP isomers. Peak assignments are discussed in the text and given in Table 1

under relatively mild conditions, RSB in solution undergoes facile 6π electrocyclization from the 12,13,14-*cis* form to give the cyclic DHP structure, according to the mechanism shown in Scheme 2 [9, 20]. Upon preparing the neutral *n*-butylamine Schiff base of 13-*cis* retinal, they found that the initial mixture contained 7% DHP, along with 8% all-*trans* and 85% 13-*cis* RSB [9]. Heating at 78 °C in C_6D_6 for 30 min produced a 2:5:3 ratio of 13-*cis* RSB, *trans* RSB, and the DHP form. The efficiency of the 6π electrocyclization process was explained by Tanaka et al. to be due to favorable HOMO-LUMO overlap for the 12,13,14-*cis* RSB form [21]. Similar 6π electrocyclization of the polyene chain has been noted for other retinal and carotene systems [7, 9, 20, 22–24].

Based on the considerations outlined above, it seems most likely that the *m/z* = 338 ion is the *N*-*n*-butyl-2-(β-ionylidene)-4-methylpyridinium cation (BIP, Scheme 1), the dehydrogenated form of the DHP structure observed by Okamura et al. [9], formed following sequential RSB cyclization, protonation, and H_2 loss in solution. Attempts to create the *m/z* = 338 ion through collisional excitation of RPSB (*m/z* = 340) in the first ion funnel or in the slammer region were unsuccessful, possibly because for kinetic reasons there is a preference for other fragmentation products. Previous studies demonstrate that the major CID product from RPSB in the gas phase is β-ionone protonated Schiff base (*m/z* = 248) + toluene [7, 8].

To link the measured collision cross sections for the *m/z* = 338 ion with molecular structures, we carried out density functional theory (DFT) calculations for different BIP isomers employing the M06-2X functional with the cc-pVDZ basis set [25]. A similar computational approach was used previously for RPSB and its isomers [7, 19]. According to the calculations, cyclization of *trans* RPSB to form *trans* BIP and H_2 is predicted to be exothermic by 25 kJ/mol. The *trans* and 9-*cis* BIP isomers are predicted to be almost isoenergetic. The barrier for isomerization around the C_9=C_{10} double bond was calculated at the DFT M06-2X/cc-pVDZ level by varying the C_8-C_9=C_{10}-C_{11} dihedral angle while allowing the rest of the structure to relax, and was found to be 120 kJ/mol with respect to *trans* BIP. Collision cross sections ($\bar{\Omega}_{calc}$) for the various BIP isomers with N_2 were estimated using the MOBCAL program

with the trajectory method [26, 27], employing appropriate parameters for N_2 buffer gas [28]. The *trans* BIP isomer is calculated to have the largest collision cross section with N_2, whereas the *cis* isomers are predicted to have ≈2% smaller cross sections. Energies and collision cross sections for the various BIP isomers are provided in Table 1.

Based on calculated isomer collision cross sections and energies, the most convincing assignment for the observed ATD peaks in Figure 2 are X = *trans* BIP, and Y = 7-*cis*, 9-*cis*, or 7,9-*cis* BIP. The calculated cross sections for *cis* BIP isomers underestimate the measured cross section for isomer Y by 1%, whereas the calculated cross section for *trans* BIP underestimates the measured cross section by 4%. These discrepancies are typical for the trajectory method predictions for cross sections for collisions between small protonated molecules and N_2. For example, the measured collision cross section for RPSB is underestimated by 5% by the trajectory method calculations. Von Helden and coworkers found that the trajectory method underestimated the collision cross section for the O protonated isomer of benzocaine by 2%, whereas the cross section of the N protonated isomer was underestimated by 7% [29].

At this stage, we are unable to determine if peak Y is attributable to a single *cis* isomer, or if it contains contributions from all three *cis* isomers. Alternative *m/z* = 338 isomers were also investigated using DFT and are considered at the end of this section (with information on energies and collision cross sections provided in the Supporting Information).

Collision-Induced Dissociation of the m/z = 338 Cation

Support for the *m/z* = 338 cation's assignment to the BIP structure was obtained through MS^n CID mass spectra (recorded using the Orbitrap as outlined in the Experimental section). Masses of the main fragment ions, their molecular formulas, the corresponding neutral fragment, and MS^n fragmentation mass spectra are summarized in Section 6 of the Supporting Information. The main fragmentation pathways are shown in Scheme 3. High resolution mass spectra show that all observed charged fragments contain an N atom, consistent with the proposed cyclic BIP structure. The *m/z* = 282 fragment (–C_4H_8) can be produced either through loss of the butyl chain or through cyclization of the polyene chain onto the ionone ring, causing ring opening and loss of C_4H_8. The smallest observed charged fragment at *m/z* = 108 has the molecular formula $C_7H_{10}N^+$, and is assigned as protonated 2,4-lutidine. This assignment is supported by the close match between the ATD of the *m/z* = 108 fragment and a reference ATD of protonated 2,4-lutidine (shown in Figure 3). Overall, the CID data are consistent with the proposed fragmentation cascade shown in Scheme 3 and the BIP structure for the *m/z* = 338 cation.

Table 1. Data for BIP and RPSB Isomers, Including M06-2X/cc-pVDZ energies relative to *trans* RPSB (corrected for vibrational zero-point energy), calculated collision cross sections with N_2, and measured collision cross sections with N_2. Calculated energies and collision cross sections are averages over the 6s-*trans*, 6s-*cis*(–), and 6s-*cis*(+) configurations as explained in the Supporting Information. A complete data compilation is given in the Supporting Information

Structure (calculated)	ΔE[a] (kJ/mol)	$\overline{\Omega}_{calc}$ (Å^2)	ATD peak	Ω_m[b] (Å^2)
BIP				
trans	–37	204.5	X	212.4
7-*cis*	–25	201.6	Y	203.8
9-*cis*	–39	201.1	Y	203.8
7,9-*cis*	–27	200.6	Y	203.8
RPSB[c]				
trans	0	219.9	A	231.9
single-*cis*	3–24	215.7–220.3	B	226.9
double-*cis*	5–44	211.7–222.7	B, C'	226.9, 214.6
triple-*cis*	23–46	197.9–209.2	C', D	214.6, 207.9
cyclic	1–63	192.1–210.1	C', D	214.6, 207.9

[a] Relative energies for BIP structures correspond to [BIP + H_2].
[b] Estimated absolute errors of ±5 Å^2 and relative errors of ±0.3 Å^2.
[c] RPSB data from refs. [18] and [19].

Photoisomerization of BIP

The photoisomerization behaviors of the X and Y isomers of the *m/z* = 338 cation were investigated through tandem IMS-photo-IMS studies. The target isomer was selected in the first stage of the IMS and irradiated with tunable light from an OPO immediately after the second ion gate (see Figure 1). Resulting photoisomers were separated from the parent isomer in the second IMS stage. The laser-on/laser-off ATDs (Figure 4) demonstrate that isomer X (assigned as the *trans* BIP isomer) is photoconverted to the more compact Y isomer (assigned as

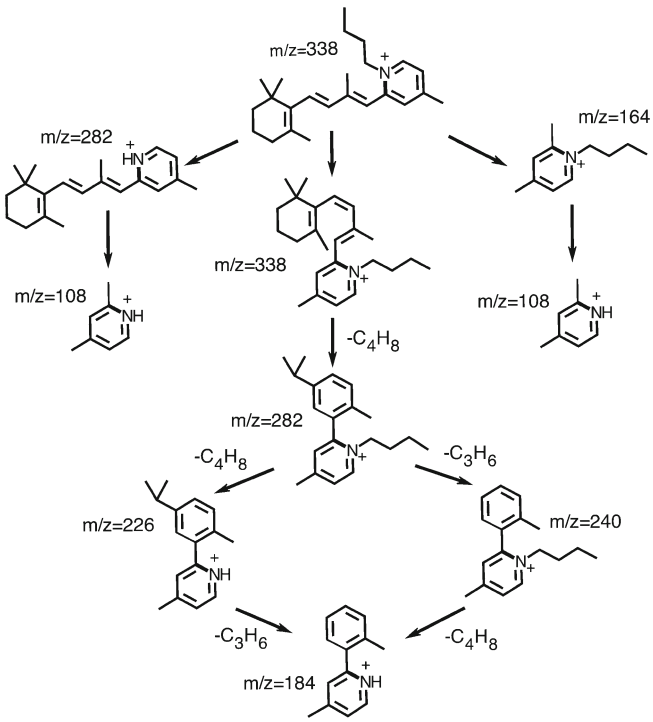

Scheme 3. Proposed collision induced dissociation pathways for the *m/z* = 338 BIP cation

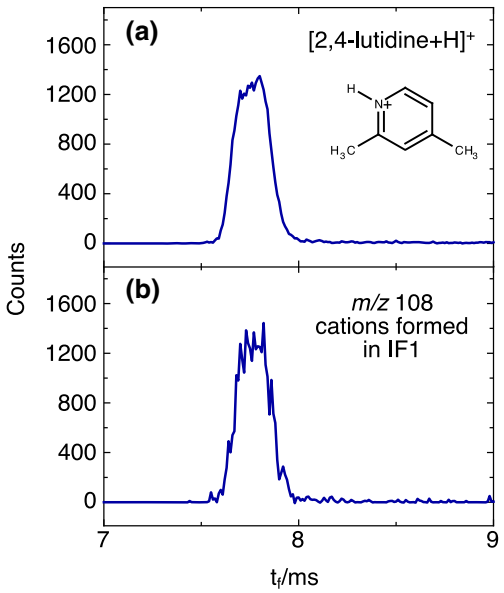

Figure 3. Arrival time distributions (P = 6.2 Torr, N_2 buffer gas) for **(a)** electrosprayed reference protonated 2,4-lutidine, and **(b)** *m/z* = 108 ions formed through collisional activation of electrosprayed ions in IF1

the *cis* BIP isomer), and vice versa. Plots of the photoisomer yield as a function of wavelength (photoisomerization action spectra) of the *trans* and *cis* BIP isomers are shown in Figure 5. The spectra of both isomers exhibit a broad band with maximum response at ≈ 420 nm. The almost identical PISA spectra for isomers X and Y are consistent with their assignment as *trans* and *cis* BIP isomers, which should have very similar electronic transitions. To confirm that the observed electronic

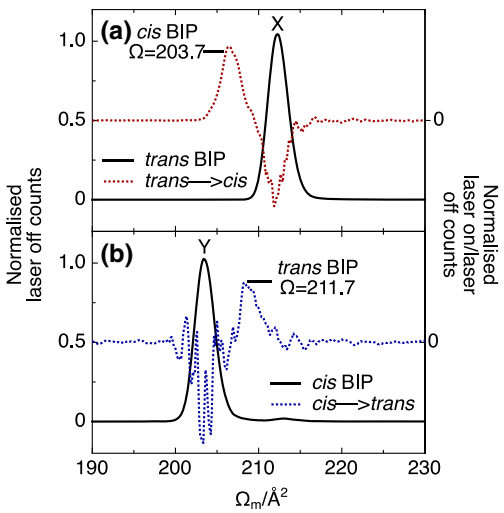

Figure 4. Arrival time distributions for mobility-selected *m/z* = 338 cations. Laser off data are shown in black, and laser on/laser off difference data are represented by blue dotted lines. Collision cross sections for photoisomers are indicated (Ω in $Å^2$). **(a)** IG2 opened to transmit isomer X, with alternate ion packets irradiated by 420 nm light. **(b)** IG2 opened to transmit isomer Y, with alternate ion packets irradiated by 420 nm light

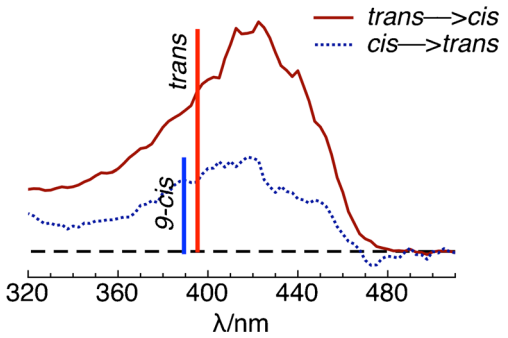

Figure 5. Photoisomerization action spectra of *trans* BIP (X) and *cis* BIP (Y). The photoisomerization response is measured as a function of wavelength, and is normalized at each wavelength by photon number. Calculated vertical excitation wavelengths and intensities (TD-DFT CAM-B3LYP/6-31+g) for *trans* and 9-*cis* BIP are shown as vertical bars

absorption bands are consistent with the *trans* and *cis* BIP isomers, we calculated vertical $S_1 \leftarrow S_0$ excitation energies using time-dependent density functional theory (TD-DFT) at the CAM-B3LYP/6-31+g level. As shown in Figure 5, the predicted vertical $S_1 \leftarrow S_0$ excitation wavelengths for *trans* and 9-*cis* BIP are 395 and 390 nm, respectively, close to the maximum of the observed PISA bands (420 nm). Furthermore, the predicted ratio of the oscillator strengths for the $S_1 \leftarrow S_0$ transitions of the *trans* and 9-*cis* isomers is 1.75, consistent with the observation that photoisomerization response for isomer X (*trans* BIP) is around twice that of isomer Y (*cis* BIP).

Collision Induced Isomerization of BIP

Having established the photoisomerization behavior of *trans* and *cis* BIP isomers, we explored their interconversion through buffer gas collisions in the slammer region. The threshold for collision induced isomerization of a mobility-selected BIP isomer was ascertained by scanning the potential difference between the slammer electrodes (from 20 to 320 V) while measuring the arrival time distribution of the resulting ions. As explained in the Supporting Information, relative abundances of the parent and daughter ions were determined at each slammer potential difference by fitting the ATD with a sum of Gaussian functions, each of which corresponds to a different isomer. The data can be analyzed in terms of three isomers, the *trans* (X) and *cis* (Y) isomers, and a more compact isomer, Z, produced in minor quantities at slammer voltages exceeding 210 V. Resulting plots of isomer intensity against slammer voltage are shown in Figure 6. As described in the Supporting Information, the breakdown curves were fitted with a sigmoidal function, where the threshold voltage (V_T) is defined as the voltage at which 3.5% of the parent ion population has undergone collision induced isomerization, or at which the relative abundance of the daughter ion population reaches 3.5%.

Threshold voltages for *trans*→*cis* isomerization (185 ± 3 V) and reverse *cis*→*trans* isomerization (190 ± 3 V) are similar, consistent with the DFT predictions of relatively small energy differences between the *trans* and 9-*cis* geometric isomers. As

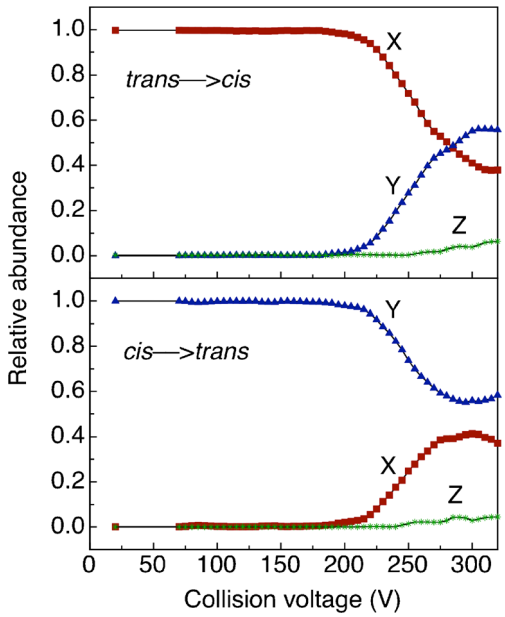

Figure 6. Breakdown diagrams for collisional isomerization of *trans* BIP (X, upper) and *cis* BIP (Y, lower). Selected *trans* or *cis* BIP isomers transmitted by IG2 were subjected to energetic collisions with N_2 buffer gas causing *cis*/*trans* isomerization. A more compact isomer, Z, was formed in minor quantities at higher voltages

noted earlier, the barrier for isomerization around the C_9=C_{10} double bond was calculated to be 120 kJ/mol with respect to *trans* BIP at the DFT M06-2X/cc-pVDZ level. Although *trans* BIP (X) is formed preferentially through electrospray ionization, at high slammer voltages (above 270 V) the *cis* isomers of BIP (peak Y) begin to dominate. Possibly, this is because the higher energy 7-*cis* and 7,9-*cis* BIP isomers are also generated at elevated collision energy. It is relevant to note that no matter if the *trans* or *cis* BIP isomer was initially selected, the relative abundance of X:Y:Z at the highest attainable slammer voltage (320 V) was 0.38:0.57:0.05, suggesting that a pseudo-equilibrium between the different isomers is reached at higher collision energies. The structure of isomer Z is uncertain, but it may correspond to the retro-γ-retinylidene cation resulting from a [1, 5] sigmatropic shift.

At very high slammer voltages, collision induced fragmentation of the *m/z* = 338 cations occurs, primarily giving the same fragment ions to those formed in the Orbitrap and LTQ CID experiments discussed previously. The *m/z* = 280 ion is particularly abundant. However, drop off in the transmission and sensitivity below *m/z* = 180 restricts our ability to detect low mass fragments.

Alternative Isomer Assignments for the m/z = 338 Cation

Here we consider possible alternative structures for the *m/z* = 338 cation, including the isomers shown in Scheme 4. Calculated M06-2X/cc-pVDZ energies and trajectory method collision cross sections for these isomers are compiled in the Supporting Information. The bicyclo-RPSB isomer is an unlikely candidate based on its high relative energy (≈ +88 kJ/mol with respect to *trans* BIP) and because it lacks the necessary conjugated network for it to absorb visible light. The 7,12-cyclo-RPSB *trans* and *cis* structures lie lower in energy and have predicted collision cross sections that are roughly consistent with the experimental cross sections for the X and Y isomers.

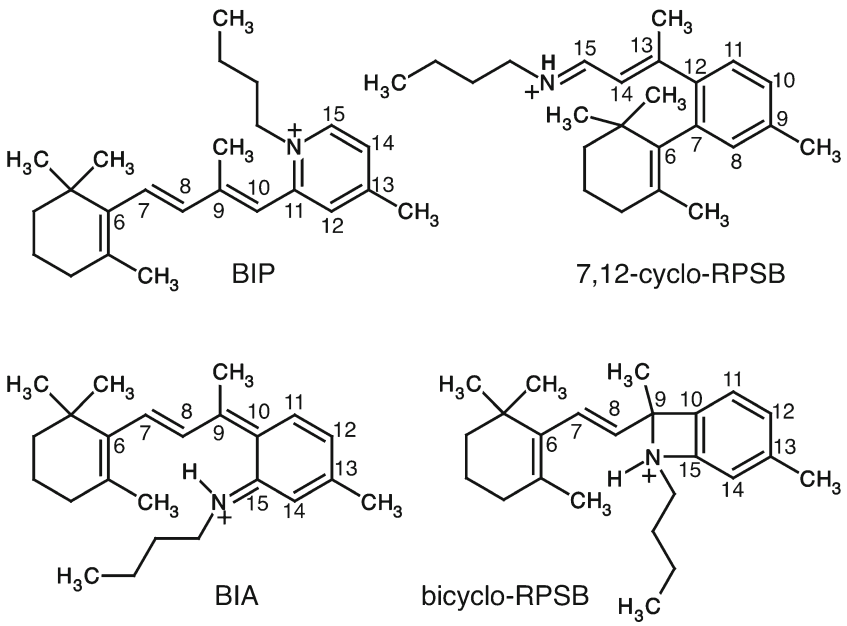

Scheme 4. Candidates for the *m/z* = 338 cation: BIP = *N*-*n*-butyl-2-(β-ionylidene)-4-methylpyridinium, BIA = *N*-*n*-butyl-2-(β-ionylidene)-4-methylanilinium

They are also expected to absorb light in a similar spectral region to BIP because of their extended conjugated structures. However, formation of the *m/z* = 108 fragment from the *m/z* = 338 cation in collision induced dissociation experiments, which is assigned as 2,4-lutidine by IMS, is difficult to rationalize for the 7,12-cyclo-RPSB molecule. Another candidate, the BIA cation, should absorb visible light and have *trans* and *cis* isomers with cross sections that are consistent with the measured cross sections for the X and Y isomers. However, formation of the precursor from retinal Schiff base cannot occur through a 6π electrocyclization and would require an unlikely process in which a single bond is established between C_{10} and C_{15} coordinated with a loss of H atoms from C_{10} and C_{15} (to liberate H_2). In contrast, previous experimental studies demonstrate facile formation of the neutral DHP molecule, the BIP precursor, through a 6π electrocyclization mechanism [9].

Conclusions

We have studied one of the main degradation products of retinal Schiff base in solution. The data suggest that RSB undergoes 6π electrocyclization to form the neutral DHP molecule, which, following protonation in solution, loses H_2 to form the BIP cation. Assignment of the observed degradation product to BIP is consistent with previous observations of the DHP structure in solution [9], and is supported by the DFT calculations, high resolution CID mass spectra, ion mobility ATDs, and photoisomerization action spectra. Significantly, BIP can be converted reversibly between *trans* and *cis* forms in the gas phase through absorption of light ($\lambda_{max} \approx 420$ nm) or through buffer gas collisions. It is possible that the reversible *cis*/*trans* photoisomerization properties BIP discovered in this study may be exploited as the core unit in new light-activated molecular machines.

Another notable aspect of the work is the use of ion mobility mass spectrometry to identify the structure of a *m/z* = 108 CID fragment from BIP as protonated 2,4-lutidine. Previously, we used a similar approach to identify the main photofragment from RPSB as the protonated Schiff base of β-ionone [7]. Using tandem IMS in this way, with either collisional or photo excitation, provides a potentially powerful route towards structural elucidation of charged molecular fragments that is less cumbersome than alternative approaches such as isotopic labeling.

Acknowledgments

This research was supported under the Australian Research Council's Discovery Project funding scheme (Project Numbers DP110100312 and DP120100100). The Australian Research Council is acknowledged for support for the Orbitrap mass spectrometer at UOW through LE120100059. The authors thank Professor Matthew Bush for providing a modified version of the Mobcal code with N_2 collision parameters described in ref. [28].

References

1. Wald, G.: Molecular basis of visual excitation. Science **162**, 230–239 (1968)
2. Oesterhelt, D., Stoeckenius, W.: Rhodopsin-like protein from the purple membrane of Halobacterium halobium. Nat. New Biol. **233**, 149–152 (1971)
3. Ernst, O.P., Lodowski, D.T., Elstner, M., Hegemann, P.: Microbial and animal rhodopsins: structures, functions, and molecular mechanisms. Chem. Rev. **114**, 126–163 (2013)
4. Fishkin, N.E., Pescitelli, G., Sparrow, J.R., Nakanishi, K., Berova, N.: Absolute configurational determination of an all-trans-retinal dimer isolated from photoreceptor outer segments. Chirality **16**, 637–641 (2004)
5. Fishkin, N.E., Sparrow, J.R., Allikmets, R., Nakanishi, K.: Isolation and characterization of a retinal pigment epithelial cell fluorophore: an all-trans-retinal dimer conjugate. Proc. Natl. Acad. Sci. **102**, 7091–7096 (2005)
6. Kim, S.R., Jang, Y.P., Jockusch, S., Fishkin, N.E., Turro, N.J., Sparrow, J.R.: The all-trans-retinal dimer series of lipofuscin pigments in retinal pigment epithelial cells in a recessive stargardt disease model. Proc. Natl. Acad. Sci. **104**, 19273–19278 (2007)
7. Coughlan, N.J.A., Adamson, B.D., Catani, K.J., Wille, U., Bieske, E.J.: Ion mobility unlocks the photofragmentation mechanism of retinal protonated Schiff base. J. Phys. Chem. Lett. **5**, 3195–3199 (2014)
8. Toker, Y., Rahbek, D.B., Kiefer, H.V., Rajput, J., Antoine, R., Dugourd, P., Nielsen, S.B., Bochenkova, A.V., Andersen, L.H.: Photoresponse of the protonated Schiff-base retinal chromophore in the gas phase. Phys. Chem. Chem. Phys. **15**, 19566–19569 (2013)
9. Okamura, W.H., de Lera, A.R., Reischl, W.: Electrocyclic reactions of 13-*cis* retinal Schiff bases. J. Am. Chem. Soc. **110**, 4462–4464 (1988)
10. Dugave, C., Demange, L.: *Cis-trans* isomerization of organic molecules and biomolecules: implications and applications. Chem. Rev. **103**, 2475–2532 (2003)
11. Katsonis, M., Lubomska, M., Pollard, M., Feringa, B., Rudolf, P.: Synthetic light-activated molecular switches and motors on surfaces. Prog. Surf. Sci. **82**, 407–434 (2007)
12. Browne, W.R., Feringa, B.L.: Light switching of molecules on surfaces. Ann. Rev. Phys. Chem. **60**, 407–428 (2009)
13. Adamson, B.D., Coughlan, N.J.A., Markworth, P.B., Continetti, R.E., Bieske, E.J.: An ion mobility mass spectrometer for investigating photoisomerization and photodissociation of molecular ions. Rev. Sci. Instrum. **85**, 123109 (2014)
14. Markworth, P.B., Coughlan, N.J.A., Adamson, B.D., Goerigk, L., Bieske, E.J.: Photoisomerization action spectroscopy: flicking the protonated merocyanine-spiropyran switch in the gas phase. Phys. Chem. Chem. Phys. **17**, 25676–25688 (2015)
15. Revercomb, H.E., Mason, E.A.: Theory of plasma chromatography/gaseous electrophoresis—a review. Anal. Chem. **47**, 970–983 (1975)
16. Pierson, N.A., Clemmer, D.E.: IMS threshold method for semiquantitative determination of activation barriers: interconversion of proline *cis*. Int. J. Mass Spectrom. **377**, 646–654 (2015)
17. Dilger, J., Musbat, L., Sheves, M., Bochenkova, A.V., Clemmer, D.E., Toker, Y.: Direct measurement of the isomerization barrier of the isolated retinal chromophore. Angew. Chem. Int. Ed. **54**, 4748–4752 (2015)
18. Coughlan, N.J.A., Catani, K.J., Adamson, B.D., Wille, U., Bieske, E.J.: Photoisomerization action spectrum of retinal protonated Schiff base in the gas phase. J. Chem. Phys. **140**, 164307 (2014)
19. Coughlan, N.J.A., Adamson, B.D., Gamon, L.F., Catani, K.J., Bieske, E.J.: Retinal shows its true colors: photoisomerization action spectra of mobility-selected isomers of retinal protonated Schiff base. Phys. Chem. Chem. Phys. **17**, 22623–22631 (2015)
20. de Lera, A.R., Reischl, W., Okamura, W.H.: On the thermal behavior of Schiff bases of retinal and its analogues: 1,2-dihydropyridine formation via six-7-electron electrocyclization of 13-*cis* isomers. J. Am. Chem. Soc. **111**, 4051–4063 (1989)

21. Tanaka, K., Mori, H., Yamamoto, M., Katsumura, S.: Significant acceleration of 6π-azaelectrocyclization resulting from a remarkable substituent effect and formal synthesis of the ocular age pigment A2E by a new method for substituted pyridine synthesis. J. Org. Chem. **66**, 3099–3110 (2001)
22. Tsukida, K., Ito, M., Kodama, A.: Electrocyclized retinal. J. Nutr. Sci. Vitaminol. **23**, 375–376 (1977)
23. Tsukida, K., Ito, M., Kodama, A.: Electrocyclization reaction of higher conjugated polyenals: photochemical behaviors of retinal (vitamin A1 aldehyde) homologues. J. Nutr. Sci. Vitaminol. **24**, 143–148 (1978)
24. van Breemen, R.B., Dong, L., Pajkovic, N.D.: Atmospheric pressure chemical ionization tandem mass spectrometry of carotenoids. Int. J. Mass Spectrom. **312**, 163–172 (2012)
25. Frisch, M.J., Trucks, G.W., Schlegel, H.B., Scuseria, G.E., Robb, M.A., Cheeseman, J.R., Scalmani, G., Barone, V., Mennucci, B., Petersson, G.A., Nakatsuji, H., Caricato, M., Li, X., Hratchian, H.P., Izmaylov, A.F., Bloino, J., Zheng, G., Sonnenberg, J.L., Hada, M., Ehara, M., Toyota, K., Fukuda, R., Hasegawa, J., Ishida, M., Nakajima, T., Honda, Y., Kitao, O., Nakai, H., Vreven, T., Montgomery Jr., J.A., Peralta, J.E., Ogliaro, F., Bearpark, M., Heyd, J.J., Brothers, E., Kudin, K.N., Staroverov, V.N., Kobayashi, R., Normand, J., Raghavachari, K., Rendell, A., Burant, J.C., Iyengar, S.S., Tomasi, J., Cossi, M., Rega, N., Millam, J.M., Klene, M., Knox, J.E., Cross, J.B., Bakken, V., Adamo, C., Jaramillo, J., Gomperts, R., Stratmann, R.E., Yazyev, O., Austin, A.J., Cammi, R., Pomelli, C., Ochterski, J.W., Martin, R.L., Morokuma, K., Zakrzewski, V.G., Voth, G.A., Salvador, P., Dannenberg, J.J., Dapprich, S., Daniels, A.D., Farkas, Ö., Foresman, J.B., Ortiz, J.V., Cioslowski, J., Fox, D.J.: Gaussian 09, Revision E.01. Gaussian, Inc, Wallingford CT (2009)
26. Mesleh, M., Hunter, J., Shvartsburg, A., Schatz, G., Jarrold, M.: Structural information from ion mobility measurements: effects of the long-range potential. J. Phys. Chem. **100**, 16082–16086 (1996)
27. Shvartsburg, A.A., Jarrold, M.F.: An exact hard-spheres scattering model for the mobilities of polyatomic ions. Chem. Phys. Lett. **261**, 86–91 (1996)
28. Campuzano, I., Bush, M.F., Robinson, C.V., Beaumont, C., Richardson, K., Kim, H., Kim, H.I.: Structural characterization of drug-like compounds by ion mobility mass spectrometry: comparison of theoretical and experimentally derived nitrogen collision cross sections. Anal. Chem. **84**, 1026–1033 (2012)
29. Warnke, S., Seo, J., Boschmans, J., Sobott, F., Scrivens, J.H., Bleiholder, C., Bowers, M.T., Gewinner, S., Schöllkopf, W., Pagel, K., von Helden, G.: Protomers of Benzocaine: Solvent and Permittivity Dependence. J. Am. Chem. Soc. **137**, 4236–4242 (2015)